

A comprehensive study on beam dynamics inside symmetrically chirped waveguide array mimicking the graded index media

Anuj P. Lara¹ and Samudra Roy^{1,*}

¹*Department of Physics, Indian Institute of Technology Kharagpur, Kharagpur 721302, India*

In this article we theoretically investigate the beam dynamics inside symmetrically chirped nonlinear waveguide arrays, while taking into account two different chirping schemes, namely linear and quadratic. We propose realistic structure of chirped waveguide array that opens up new avenues in controlling the light flow. The beam dynamics inside such waveguides are modeled by adopting a continuous approximation of the discrete nonlinear Schrödinger equation (DNLSE) that usually governs the beam propagating in a discrete system which facilitates us in applying the semi-analytical variational method to grasp the beam dynamics. Our analytical treatment reveals that the symmetrically chirped waveguide array unambiguously mimics the graded index system where coupling coefficient with transverse variation play an equivalent role to that of the refractive index in continuous dispersive media. Exploiting the results of variational treatment we obtain state solutions and examine their robustness from the linear stability analysis. We reveal, that a symmetrically chirped waveguide array offers an oscillatory path for an input Gaussian beam exactly like a parabolic index media, along with self-focusing and imaging of the beam under Kerr-nonlinearity. We demonstrate that, under nonlinearity, discrete solitons with sech-type shape are formed. These discrete solitons are robust and flow inside the waveguide array with a unique oscillatory trajectory as exactly predicted in our theoretical calculations. We perform a rigorous analysis to unfold the propagation characteristics of the beams in both linear and nonlinear regimes in the proposed systems and validate our results with full numerical simulations. Our investigation shed light on the complex dynamics of an optical beam and its manipulation inside a geometrically engineered chirped waveguide array.

I. INTRODUCTION

Over the decades, waveguide arrays (WAs) have proven to be a versatile photonic platform for various applications in optical communications along with the study of fundamental physics in an optical analogue. These arrays formed by the periodic arrangement of waveguide channels, allow unique optical dynamics in the macroscopic scale, which were erstwhile limited to atomic and molecular scales. Mimicking of electron like behavior of Bloch oscillations [1, 2], Peierls-Nabbaro potential [3], Anderson localization [4] which are fundamental in crystal lattices have been reported in WAs. This analogue have also been extended to relativistic phenomena like Klein tunneling [5] *Zitterbewegung* [6, 7], neutrino oscillation [8], tachyon condensation [9], classical analogues of quantum coherence, displaced Fock states [10, 11], Dirac solitons [12], etc. In addition, the formation of stable higher dimension solitons and light bullets [13–15] are achieved in these WAs along with the realization of surface [16] and vortex solitons [17]. Beam routing, steering [18–21], and lensing [22] are also successfully demonstrated in modulated photonic arrangements. In recent years, WAs as a system has also garnered attention due to the possibility of its applications in versatile platforms including parity-time (PT) symmetry [23–25], topology [26, 27], multiplexing [28] and demultiplexing [29], synthetic absorbers [30] and lasing [31]. Further advances have been

made in terms of contemporary applications in the field of quantum communications as programmable quantum circuits [32], and for the generation and distribution of entangled photons [33–35].

Many of the different applications of WAs are in fact achieved by introducing perturbations and modulations, both ordered and disordered, in to the periodic structure. For example, the disordered modulations in the WA leads to the optical analogue of Anderson localization [4, 36]. Whereas ordered systemic perturbations assist topological and non-Hermitian effects [25, 26] and *Zitterbewegung* [6] in the WA. Chirping is another form of ordered modulation in a WA where a transverse gradient in the propagation constant is introduced by means of electro [37] and thermo-optic [1] effects. Similar chirping effect can also be realized by modifying the geometry through femto-second laser waveguide writing [18] or fragmenting the waveguide geometry [38]. Such chirping is proven to be the effective way in structuring the light through beam routing [20, 39] and lensing [22, 40] that emulates a parabolic index profile.

In this present article, we primarily investigate the beam dynamics inside symmetrically chirped one dimensional nonlinear WAs. Two different chirping schemes are considered for our study, namely (i) *linear* and (ii) *quadratic*. In linearly and quadratic chirped WA, separation between two adjacent waveguide channels respectively varies in a linear and quadratic fashion in the transverse direction while keeping the arrangement symmetric about the central waveguide ($n = 0$). For such chirped WAs, we first establish a framework to obtain the functional forms of the coupling coefficient that varies in the

* samudra.roy@phy.iitkgp.ac.in

transverse direction. We utilized these expressions to derive the approximated continuous form of the discrete coupled mode equations (CME) that leads to the continuous *paraxial wave equation* and the *nonlinear Schrödinger equation* (NLSE) under low and high power regimes, respectively. Derivation of the continuous counterpart of the CME reveals that, the additional terms that appear due to the chirping in the WA, acts as an effective potential and also modifies the diffraction characteristics. Employing the semi-analytical variational technique for the 1D paraxial wave equations we obtain the expressions for the evolution of Gaussian beams for both the chirping schemes that mimic beam evolution in the continuous graded index media. Inspired by the results already established in a graded index fiber, we perform an analysis to obtain a stationary solution and self-focusing beam filamentation in our discrete system. Extending this work for high powers where Kerr effect is not negligible we perform an analysis to capture the dynamics of a discrete soliton. We theoretically predict the oscillatory dynamics of such soliton inside the symmetrically chirped WA. We validate all our analytical results by comparing them with full numerical simulation and find a satisfactory agreement. The results reveal crucial and unique features of beam dynamics inside an engineered waveguide arrangement never explored before.

II. THEORY

In order to study the beam dynamics inside a WA, we consider a semi-infinite array of identical nonlinear waveguides that are weakly coupled with their nearest neighbor by the means of evanescent coupling. We consider these waveguides to be ideal without any deformations or losses. The evolution of the mode amplitude in the n^{th} waveguide under the continuous-wave excitation with nearest-neighbor evanescent coupling is described by the coupled mode equation, formally known as the *discrete nonlinear Schrödinger equation* (DNLSE) [3, 41–44]:

$$i\frac{dE_n}{dz} + C_n^{n+1}E_{n+1} + C_n^{n-1}E_{n-1} + \gamma|E_n|^2E_n = 0. \quad (1)$$

Here E_n is the electric field amplitude in the n^{th} waveguide, C_n^{n+1} and C_n^{n-1} represent the coupling coefficients of the n^{th} waveguide to its nearest neighbors $(n+1)^{\text{th}}$ and $(n-1)^{\text{th}}$ waveguides, respectively, and γ being the nonlinear coefficient arising due to Kerr effect. For an analytical study, it is beneficial to use a normalized form of Eq. (1) by making the transformations, $\eta_n^{n+1} \rightarrow C_n^{n+1}/C_0^1$, $\xi \rightarrow C_0^1 z$, $E_n \rightarrow \sqrt{P_0}a_n$, and $\mathcal{N}^2 \rightarrow \gamma P_0/C_0^1$ to obtain,

$$i\frac{da_n}{d\xi} + \eta_n^{n+1}a_{n+1} + \eta_n^n a_{n-1} + \mathcal{N}^2|a_n|^2a_n = 0. \quad (2)$$

Here, P_0 is the peak beam power, and C_0^1 is the coupling coefficient between the $n=0$ and $n=1$ waveguides that

acts as a reference coupling coefficient or in other words the coupling coefficient in absence of any chirping. \mathcal{N} is equivalent to the soliton order in the case of the optical pulses, where $L_{NL} = 1/\gamma P_0$ is the nonlinear length [45].

For a uniform waveguide array, i.e. uniform coupling coefficients $\eta_{n-1}^n = \eta_n^{n+1} = \eta$, Eq. (2) reduces to

$$i\frac{da_n}{d\xi} + \eta(a_{n+1} + a_{n-1}) + \mathcal{N}^2|a_n|^2a_n = 0, \quad (3)$$

exhibiting a sech soliton-like solution for $\mathcal{N} = 1$ [42, 43]. In a linear WA, under low power conditions, for a discrete plane wave $a_n(\xi) = a_0 \exp[i(n\kappa + \beta\xi)]$, one obtains the well established dispersion relation between the propagation constant (β) and transverse (κ) wavenumbers, as $\beta(\xi) = 2\eta \cos(\kappa)$. Under this dispersion relation, the general solution for the propagating discrete soliton is established as [46]

$$a_{\text{sol}}(\xi, n) = a_0 \operatorname{sech} \left[\frac{na_0}{\sqrt{2\eta \cos(\kappa_0)}} \right] e^{ia_0^2\xi/2}, \quad (4)$$

where a_0 and κ_0 are the initial values of the soliton amplitude and central transverse wavenumber, respectively.

A. Waveguide array design

To design a system that can support a discrete soliton, we consider the facility of femto-second laser based waveguide writing in a transparent bulk medium [47–50], and propose an index array formed by 1.8 % GeO₂ doped silica cores suspended in a silica cladding. At the operating wavelength of $\lambda_0 = 1.55 \mu\text{m}$, the core and cladding refractive indices are found to be $\mu_1 = 1.4477$ and $\mu_2 = 1.4446$, respectively [51]. We consider the cylindrical cores to have a radius of $R = 6 \mu\text{m}$ and Kerr coefficient as $n_2 \approx 2.7 \times 10^{-20} \text{ m}^2\text{W}^{-1}$. This n_2 leads to the nonlinear coefficient for the fundamental mode as $\gamma = \omega_0 n_2 / c A_{\text{eff}} = 0.64 \text{ W}^{-1} \text{ km}^{-1}$, where ω_0 is the operating frequency and A_{eff} represents the effective mode area of the guided channel [45]. For such an array of cylindrical waveguides, the coupling coefficient between two adjacent channels is given as [52]

$$C = \frac{\lambda_0}{2\pi\mu_1} \frac{U^2}{R^2 V^2} \frac{K_0(Wd/R)}{K_1^2(W)}. \quad (5)$$

Here, d is the separation between the two waveguide channels; λ_0 is the free space wavelength (1.55 μm in this case); a is the core radius; K_j are the modified Bessel functions of the second kind of order j . U and W are the transverse mode parameters that satisfy $U^2 + W^2 = V^2$, where the V parameter is defined as $V = (2\pi R \sqrt{\mu_1^2 - \mu_2^2})/\lambda_0$. U is approximated as $U \approx 2.405e^{-(1-v/2)/V}$, with $v = 1 - (\mu_2/\mu_1)^2$ [53]. For a reference separation of $d = 30 \mu\text{m}$ we obtain a coupling coefficient of $C = 3.26 \text{ m}^{-1}$ that can support a

fundamental discrete soliton ($\mathcal{N}^2 = 1$) with a peak beam power of $P_0 = C/\gamma \approx 5.6$ kW. Note, a chirped WA is achieved by either modulating the material properties of the individual waveguides by electro/thermo-optic effects [1, 37, 54], or changing the geometry of the waveguides or the WA altogether [20, 22, 55, 56]. Eq. (5) suggests that a chirping in the inter-waveguide separation (d) leads to change in only the coupling coefficient keeping other parameters like propagation constant and nonlinear coefficients unchanged.

1. Linear Chirping

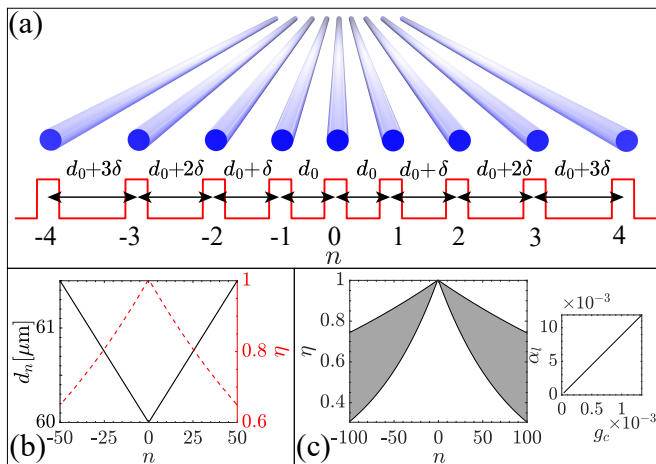


FIG. 1. (a) Schematic representation of the waveguide arrangement under a symmetric linear chirp, along with the variation in refractive index in the transverse direction. (b) The variation in the inter-waveguide separation d_n (solid black line) and the corresponding normalized coupling coefficient η (dashed red line) as a function of n , for typical parameters $\delta = 30$ nm and $d_{\text{ref}} = 30$ μm . (c) Variation of the coupling coefficient η along the transverse coordinate n for the chirping strength δ ranging from 10 nm to 40 nm (shaded region). In the right inset we plot α_l as a function of g_c .

A linearly chirped WA is described by a linear increase in the separation between the adjacent waveguides along the transverse direction. This chirping can be implemented as a function of the waveguide number or index (n) as d_n where d_n is the separation between the $(n+1)^{\text{th}}$ and n^{th} waveguides in the array, while keeping the entire arrangement symmetric about the central waveguide, i.e. $d_n = d_{-(n+1)}$ for $n = 0$. This geometric arrangement can be achieved by considering the separation between two adjacent waveguide as $d_n = d_{\text{ref}} + \delta |n + 1/2|$, with $d_0 = d_{-1} = d_{\text{ref}} + \delta/2$, where δ is called the *chirping strength*, and d_{ref} is *reference separation* which is essentially the separation between two adjacent waveguide in absence of any chirping (i.e $\delta = 0$). A schematic description of this linearly chirped symmetric WA is illustrated in Figure 1 (a), with the inset describing the variation in the refractive index along the transverse direction of the

WA. The resulting change in the waveguide separation as a function of n is shown for an array of 101 waveguide in Figure 1 (b). In the same plot we also present the corresponding normalized coupling coefficients η_n^{n+1} obtained from Eq. (5). This profile is obtained for typical parameters $\delta = 30$ nm and $d_{\text{ref}} = 30$ μm . For a fixed waveguide geometry, the variation of η depends on the chirping strength δ as seen in Figure 1 (c) where the upper and lower boundaries of the shaded area corresponds to $\delta = 10$ nm and $\delta = 40$ nm, respectively, and the shaded area depicts the intermediate δ values.

The exponentially decreasing behavior of the coupling coefficient with transverse variable n can be attributed to the exponentially decaying nature of the K_0 function and corroborates well with experiments [47]. For the considered parameters, the modified Bessel function in Eq.(5) can be approximated as $K_0(x) \approx \sqrt{\frac{\pi}{2x}} e^{-x}$, where $x = Wd_n/R$. Since we consider a weak chirping value, i.e. $\delta \ll d_0$, the variation in the denominator is negligible in comparison to the numerator, and the variation in the coupling coefficient can be approximated as $C_n^{n+1} \approx C_0^1 e^{-\alpha_l |n+1/2|}$, where $\alpha_l = mg_c$, with $m = Wd_{\text{ref}}/R$, and $g_c = \delta/d_{\text{ref}}$. The parameter g_c denotes the normalized chirping strength. The variation of the normalized coupling coefficient ($\eta_n^{n+1} = C_n^{n+1}/C_0^1$) can mathematically be fitted by the function $e^{-\alpha_l |n+1/2|}$ and one can extract the numeric value of α_l . For each value of g_c , one could obtain α_l that changes linearly as demonstrated in the inset of Figure 1 (c). For the given geometry, g_c and α_l follows a linear relationship with a slope $m = 8.7$ that corroborate well with the actual value $m = Wd_0/R \approx 8.6$.

2. Quadratic Chirping

The other chirping scheme that we consider is a symmetric quadratic chirping, where the separation between the waveguide channels vary as a quadratic function along the transverse direction. For such chirping, the inter-waveguide separation can be defined as $d_n = d_{\text{ref}} + \delta(n + 1/2)^2$, with $d_0 = d_{-1} = d_{\text{ref}} + \delta/4$. This chirping arrangement is schematically presented in Figure 2 (a), where we also demonstrate the transverse refractive index profile. The resulting variation in separation (d_n) as a function of the waveguide index (n) is given in Figure 2 (b). In the same plot we depict the corresponding coupling coefficient (red dashed line) which is obtained by using Eq. (5) for $d_{\text{ref}} = 30$ μm . The variation of η for different chirping strengths δ is presented in Figure 2(c) for upper and lower boundaries corresponding to $\delta = 0.05$ nm, and 0.25 nm, respectively. The variation of the coupling coefficient along n is approximately obtained by fitting the functional form as $\eta_n^{n+1} \approx e^{-\alpha_q (n+1/2)^2}$, where α_q is the coefficient of quadratic chirping. The numerical plots for $\eta(n)$ given in Figure 2 (c) obtained from Eq. (5) is in good agreement with the approximate expres-

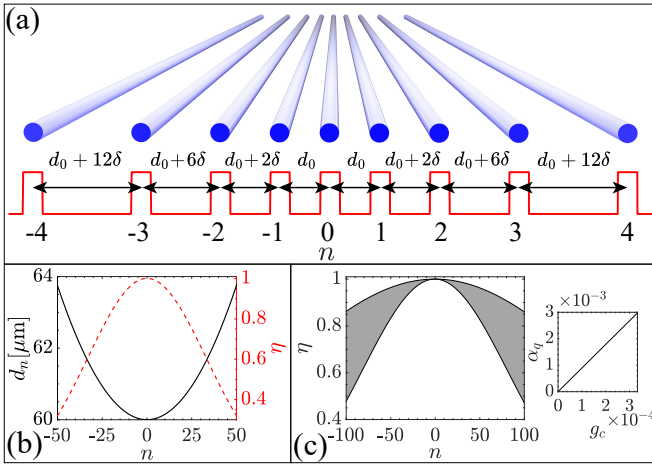


FIG. 2. (a) Schematic representation of the waveguide arrangement under a symmetric quadratic chirp, along with the variation in refractive index in the transverse direction. (b) The variation of d_n , the separation between adjacent waveguides, (solid black line) and the corresponding normalized coupling coefficient profile η (dashed red line) for $\delta = 1.5$ nm along the transverse coordinate n . (c) Variation of the coupling coefficient η along the transverse coordinate n for the chirping strength δ ranging from 0.05 nm to 0.25 nm (shaded region). In the right inset we plot α_q as a function of g_c .

sions where α_q and g_c follows the same linear relationship $\alpha_q = mg_c$ [Figure 2 (c) inset] with $m \approx 8.7$. Hence, in summary, we define an explicit functional form of the coupling coefficient $\eta(n)$ for both the chirping schemes in terms of an exponential function of n and the normalized chirping strength g_c . In the following section we exploit these approximated functional form to establish the continuous counterpart of the DNLSE.

B. Continuous approximation of the DNLSEs

In this present work, we put forward an analytical proposal based on the variational technique [57] to approximately solve Eq. (2), the DNLSE. The discrete nature of the WA raises a challenge to apply the analytical treatment which can be resolved by considering continuous approximation of the transverse variable (n). Such an approximation is justified when the beams under consideration usually encompass many waveguides (> 5) [42, 46]. Assuming the mode distribution as a continuous function of n one can make the transformation as $a_n(\xi) \rightarrow \psi(n, \xi)$. Now expanding the nearest neighbour mode by Taylor expansion [42] we have,

$$\psi(n \pm 1, \xi) = \psi(n, \xi) \pm \partial_n \psi(n, \xi) + \frac{1}{2} \partial_n^2 \psi(n, \xi). \quad (6)$$

Incorporating these modifications in Eq. (2), we obtain the continuous counterpart of the DNLSE as,

$$i\partial_\xi \psi + |\psi|^2 \psi + \left(\eta_n^{n+1} + \eta_n^n \right) \left[\psi + \frac{1}{2} \partial_n^2 \psi \right] + \left(\eta_n^{n+1} - \eta_n^n \right) \partial_n \psi = 0. \quad (7)$$

Note, the information of the waveguide chirping (i.e. linear or quadratic) is embedded in the coupling coefficients η_n^{n+1} and η_n^n . For example, in case of linear chirping we have $\eta_n^{n+1} = e^{-\alpha_l |n+1/2|}$. For small values of α_l ($\approx 10^{-3}$), and assuming the fact that the beams remain confined within $-50 < n < 50$, we can approximate the DNLSE as (for details see Appendix A),

$$i\partial_\xi \psi + \partial_n^2 \psi + 2\psi + \mathcal{N}^2 |\psi|^2 \psi = \alpha_l |n| \left(2\psi + \partial_n^2 \psi \right) + \text{sgn}(n) \alpha_l \partial_n \psi. \quad (8)$$

Similarly, under the quadratic chirping scheme where the coupling coefficient is approximately written in the functional form $\eta_n^{n+1} = e^{-\alpha_q (n+1/2)^2}$, the effective DNLSE is obtained as,

$$i\partial_\xi \psi + 2\psi + \partial_n^2 \psi + \mathcal{N}^2 |\psi|^2 \psi = \alpha_q n^2 \left(2\psi + \partial_n^2 \psi \right) + 2\alpha_q n \partial_n \psi. \quad (9)$$

The three terms shown in the RHS of Eq.(8) and Eq.(9) are originated due to the chirping in the WA. The first term represents an effective potential and the most dominant among all three. Physically, the second term introduces a gradient in diffraction coefficient and the third term accounts for the transverse motion due to asymmetry in the coupling coefficient. Note, the shape of potentials are triangular and parabolic for linear and quadratic chirping with a strength of $2\alpha_{l,q}$.

To ensure the correctness of the derived NLSE Eq.(8) and Eq.(9) we solve both of them numerically. For our numerical simulation we consider the input as the discrete soliton with the following form [46],

$$a_n = \psi_0 \text{sech} \left[\frac{\psi_0 (n - n_0)}{\sqrt{2\eta \cos(\kappa_0)}} \right] e^{i[\phi + \kappa_0 (n - n_0)]}, \quad (10)$$

where ψ_0 , n_0 , ϕ , and κ_0 are the soliton parameters that can evolve with ξ . The soliton dynamics with the initial conditions of $\psi_0(0) = 0.5$, $n_0(0) = 15$, $\kappa_0(0) = 0$, and $\phi(0) = 0$ for both the chirping schemes are demonstrated in Figure 3. We obtain the results by solving the DNLSE (Eq. (2)) and its continuous counterpart (Eq.(8) and Eq.(9)).

For our simulation $\delta = 10$ nm and 0.5 nm are taken as the strengths of the linear (see Figure 3 (i)) and quadratic chirping (see Figure 3 (ii)), respectively. We emphasize that, an excellent agreement is observed when we numerically solve the fundamental DNLSE and its approximated continuous counterpart (Eq.(8) and Eq.(9)) that we developed. The variation of different soliton parameters

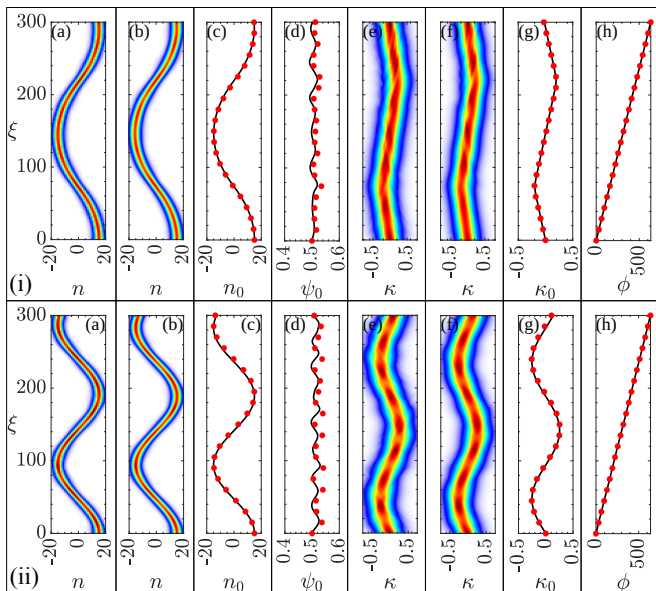


FIG. 3. Comparison of a soliton evolving as per the DNLS and the approximate NLSE under (i) linear and (ii) quadratic chirping. (a) and (b) are the evolution in n space along with the corresponding evolution in the wavenumber (κ) space (e) and (f) as per the DNLS and NLSE, respectively. The evolution of the parameters as per the DNLS (solid red dots) and NLSE (solid black line) are given in (c) n_0 , (d) ψ_0 , (g) κ_0 , and (h) ϕ .

that we capture through numerical process for two different governing equations are also found to be compatible (see Figure 3 (i),(ii) (c),(d),(g),(h)). This comprehensive numerical exercise validates the correctness of the governing equation that we derive in Eq.(8) and Eq.(9) and provide us a concrete platform to employ the variational treatment that can unfold the complex dynamic of DS inside a chirped WA.

III. VARIATIONAL ANALYSIS AND RESULTS

In the previous section we derive a continuous counterpart of the fundamental DNLS which facilitates the use of VA in the chirped WA problem. Based on the beam powers, we may split our study into two parts (a) linear domain (for low power) and (b) nonlinear domain (for high power). In the linear domain we neglect the nonlinear effect by removing the SPM term from the governing equation and study the evolution of a Gaussian beam for two chirping schemes. We aim to establish the condition to get a stationary solution supported by these chirped WAs. In the nonlinear domain a soliton like solution can be achieved with typical *sech* form for uniform WA [46]. Considering a *sech ansatz* we perform a VA to unfold the behavior of the propagating solitonic beam where waveguide chirping behave as a perturbation.

A. Linear Case (in absence of nonlinearity)

In the regime of low powers, the self-phase modulation term can be neglected ($\mathcal{N}^2 \rightarrow 0$) and for the linearly chirped WA the NLSEs Eq. (8) can be written as,

$$i\partial_\xi\psi + \partial_n^2\psi + 2\psi - \alpha_l|n| \left(2\psi + \partial_n^2\psi \right) - \text{sgn}(n)\alpha_l\partial_n\psi = 0. \quad (11)$$

Similarly for the case of quadratic chirping Eq.(9) can be rearranged as,

$$i\partial_\xi\psi + \partial_n^2\psi + 2\psi - \alpha_q n^2 \left(2\psi + \partial_n^2\psi \right) - 2\alpha_q n\partial_n\psi = 0. \quad (12)$$

To proceed with the variational treatment first we construct the Lagrangian density \mathcal{L} for each of these governing equations (i.e. Eq. (11) and Eq. (12)) followed by an appropriate *ansatz* that reduces the Lagrangian as, $L = \int_{-\infty}^{\infty} \mathcal{L}dn$. Adopting the standard Rayleigh-Ritz optimization [57], we formulate the *Euler-Lagrange* equation as $\partial_\xi(\partial_{\nu_\xi}L) - \partial_\nu L = 0$, where ν represents different the beam parameters (beam amplitude, width, phase-front curvature, phase etc.). The given *Euler-Lagrange* equation leads to a set of coupled ordinary differential equation (ODE) expressing the beam dynamics. For linear case, where the nonlinearity is neglected, we consider a Gaussian beam distribution as our *ansatz* in the following explicit form,

$$\psi = \psi_0 \exp \left[-\frac{n^2}{2n_w^2} + i\phi + i\theta n^2 \right], \quad (13)$$

where the beam parameters, amplitude (ψ_0), width (n_w), phase (ϕ), and phase front curvature (θ) are allowed to vary with propagation distance. Note that, for VA we assume that the shape of the propagating beam doesn't change much which is a major approximation to apply the VA.

1. Linear Chirping

In case of linear chirping, we construct the Lagrangian density corresponding to Eq. (11) as,

$$\begin{aligned} \mathcal{L} = & \frac{i}{2} (\psi\partial_\xi\psi^* - \psi^*\partial_\xi\psi) + |\partial_n\psi|^2 - 2|\psi|^2 \\ & + \alpha_l|n| \left(2|\psi|^2 - |\partial_n\psi|^2 \right). \end{aligned} \quad (14)$$

We then reduce this Lagrangian density by inserting the Gaussian *ansatz* given in Eq. (13) and obtain,

$$\begin{aligned} L = & \sqrt{\pi}\psi_0^2 \left[\frac{\alpha_l}{\sqrt{\pi}} \left(-4n_w^4\theta^2 + 2n_w^2 - 1 \right) \right. \\ & \left. + \frac{n_w^3}{2} \left(\theta' + 4\theta^2 \right) + n_w \left(\phi' - 2 \right) + \frac{1}{2n_w} \right], \end{aligned} \quad (15)$$

where the prime represents derivative with respect to ξ . Employing the *Euler-Lagrange* equations for the parameters $\nu = \psi_0, n_w, \theta$, and ϕ , we can obtain the set of coupled ODEs expressing the variation of the individual parameter during the propagation inside the linearly chirped WA.

$$d_\xi \psi_0 = \left(\frac{2\alpha_l}{\sqrt{\pi}} n_w - 1 \right) 2\psi_0 \theta \quad (16a)$$

$$d_\xi n_w = - \left(\frac{\alpha_l}{\sqrt{\pi}} n_w - 1 \right) 4n_w \theta \quad (16b)$$

$$d_\xi \theta = \frac{1}{n_w^4} - 4\theta^2 + \frac{\alpha_l}{\sqrt{\pi}} \left(12n_w \theta^2 - \frac{2}{n_w} - \frac{1}{n_w^3} \right) \quad (16c)$$

$$d_\xi \phi = 2 - \frac{1}{n_w^2} + \frac{\alpha_l}{\sqrt{\pi}} \left(\frac{3}{2n_w} - n_w - 2n_w^3 \theta^2 \right) \quad (16d)$$

We are seeking for a steady state solution which we can obtain by making Eq. (16a) and Eq. (16b) zero. One can achieve this condition for $\theta = 0$ throughout the propagation. In other words, $d_\xi \theta = 0$ and $\theta(0) = 0$. Applying these conditions in Eq. (16c) we obtain a cubic equation for the beam width (n_w) as, $n_w^3 + \frac{1}{2}n_w - \frac{\sqrt{\pi}}{2\alpha_l} = 0$, which has one real root,

$$n_w = n_{sol} = -\frac{1}{\tau^{1/3}} + \frac{\tau^{1/3}}{6}, \quad (17)$$

where $\tau = 6 \left(h + \sqrt{6 + h^2} \right)$ with $h = 9\sqrt{\pi}/\alpha_l$. The pair of imaginary roots are ignored as beam width has to be real and positive. The evolution of a Gaussian beam with the aforementioned width (see Eq. (17)) and an unit amplitude of $\psi_0 = 1$ is demonstrated in Figure 4 (a) for $\alpha_l = 3 \times 10^{-3}$. The launched beam is found to be almost stationary with minor variation in its amplitude. This variation arises due to the fact that the given Gaussian function is not the exact solution of the linearly chirped WA and hence changes its shape during propagation violating the fundamental assumption of VA. The stationary solution of the system, however, can be numerically derived considering the solution in the form $a_n(\xi) = u(n)e^{i\beta\xi}$, where β is the propagation constant, and $u(n)$ is the real mode amplitude distribution which satisfies the couple mode equation,

$$-\beta u(n) + \eta_n^{n+1} u(n+1) + \eta_{n-1}^n u(n-1) = 0. \quad (18)$$

One can solve this equation numerically for the appropriate η_n^{n+1} to obtain the stationary solution $u(n)$ and feed this as an input in the linear propagation equation (see Eq. (2)) with $\mathcal{N} = 0$. In Figure 4(b) we illustrate the stationary propagation of the beam. In Figure 4(c) we compare the shape between proposed Gaussian *ansatz* and numerically obtained stationary solution of Eq. (18) where in the inset the degree of mismatch ($\Delta|\psi|$) is shown. It can be noticed that the marginal difference between two solutions causes discrepancy in the results as depicted in Figure 4(d)-(g). In Figure 4(d)-(g) we plot the evolution of the beam parameters (under

stationary condition) obtained from the governing CME (solid red dots) and the predictions of the VA (solid lines) along with full numerical solution (blue circles). The results are in close agreement. In conclusion, by adopting the VA we approximately predict the stationary solution for a linearly chirped WA.

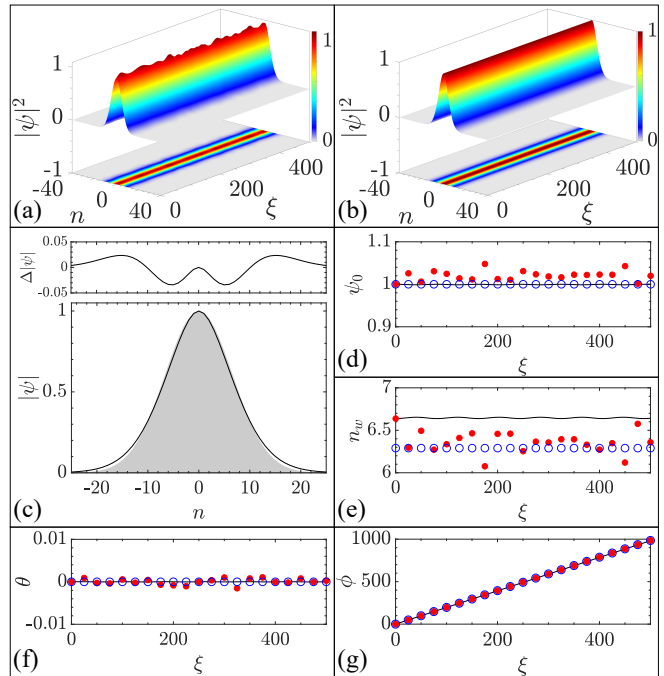


FIG. 4. Evolution of (a) a Gaussian beam having width $n_{sol} = 6.65$ and (b) the numerical solution for the CMEs in a linearly chirped WA under low power conditions for $\delta = 10$ nm. In plot (c) we superimpose the Gaussian beam shape with the numerical stationary solution of Eq. (18). In upper inset we demonstrate how much these two shapes differ. Plot (d)-(g) depict the evolution of beam parameters where the solid line represents the variation predictions. The circle and solid dots represent the corresponding values obtained from the numerical stationary solution and Gaussian feed in respectively.

2. Quadratic Chirping

We extend our investigation to quadratic chirped WA, for which the Lagrangian density can be constructed for Eq. (12) as,

$$\begin{aligned} \mathcal{L} = & \frac{i}{2} (\psi \partial_\xi \psi^* - \psi^* \partial_\xi \psi) + |\partial_n \psi|^2 - 2|\psi|^2 \\ & + \alpha_q n^2 \left(2|\psi|^2 - |\partial_n \psi|^2 \right). \end{aligned} \quad (19)$$

For a Gaussian *ansatz* (see Eq. (13)), the reduced Lagrangian is derived as,

$$L = \sqrt{\pi}\psi_0^2 \left[\alpha_q \left(-3n_w^5\theta^2 + n_w^3 - \frac{3}{4}n_w \right) + \frac{1}{2}n_w^3 (\theta' + 4\theta^2) + n_w (\phi' - 2) + \frac{1}{2n_w} \right]. \quad (20)$$

Again applying the *Ritz's optimization*, we obtain the evolution of beam parameters $\nu = \psi_0, n_w, \theta$, and ϕ in the following coupled ODE form,

$$d_\xi \psi_0 = (3\alpha_q n_w^2 - 2) \psi_0 \theta \quad (21a)$$

$$d_\xi n_w = - (3\alpha_q n_w^2 - 2) 2n_w \theta \quad (21b)$$

$$d_\xi \theta = (3\alpha_q n_w^2 - 1) 4\theta^2 + \frac{1}{n_w^4} - 2\alpha_q \quad (21c)$$

$$d_\xi \phi = 2 - \frac{1}{n_w^2} + \frac{3\alpha_q}{4} - 3\alpha_q n_w^4 \theta^2 \quad (21d)$$

For the quadratic chirped WA we can also find a stationary solution by making $d_\xi \theta = 0$ with the boundary condition $\theta(0) = 0$ in Eq. (21c) which leads to the beam width value,

$$n_w = n_{sol} = \left(\frac{1}{2\alpha_q} \right)^{1/4}. \quad (22)$$

In Figure 5 (a) we demonstrate the evolution of a Gaussian beam with unit magnitude for the width n_{sol} that we derived in Eq. (22). The plot shows a stationary propagation that corroborate well with full numerical solution depicted in Figure 5 (b). The proposed Gaussian beam is found to be a suitable *ansatz* for the WA having symmetric quadratic chirping in its arrangement. This can be validated by the comparison plot Figure 5 (c) where the proposed Gaussian function almost superimposes with the actual solution of the system that is derived numerically by solving Eq. (18). The degree of mismatch ($\Delta|\psi|$) is almost zero (see inset of plot (c)) and this exquisite matching makes the VA extremely effective specially for quadratic chirped WA. Figure 5(d)-(g) demonstrate the evolution of the beam parameters (under stationary condition) obtained from the governing CME (solid red dots) and the predictions of the VA (solid lines) along with full numerical solution (blue circles).

While, we have utilized VA to determine the stationary solution in two types of chirped WA, these results further describe the evolution of beams with arbitrary initial conditions. The evolution of Gaussian beams with unit magnitude and an arbitrary initial width of $n_w(0) = 7$ under linear and quadratic chirping are demonstrated in Figure 6 (a) and (b) respectively. The evolution of the beam parameters are also showcased in the same plot with the comparison of numerical and analytical results. VA is found to be more accurate in case of quadratic chirp WA

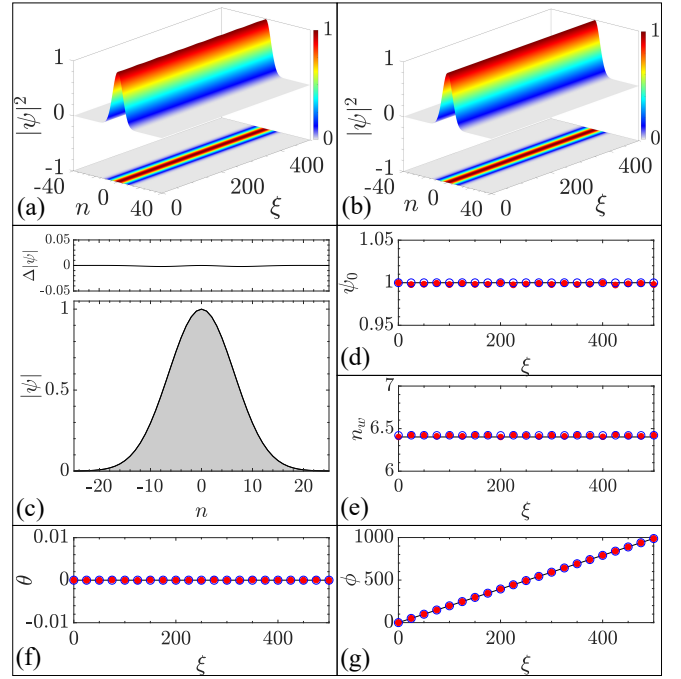


FIG. 5. Evolution of (a) an Gaussian beam having width $n_{sol} = 6.4$ and (b) the numerical solution for the CMEs in a quadratic chirped WA under low power conditions for $\delta = 1$ nm ($\alpha_q = 3 \times 10^{-4}$). In plot (c) we superimpose the Gaussian beam shape with numerical stationary solution of Eq. (18). In upper inset we demonstrate how much these two shapes differ. Plot (d)-(g) depict the evolution of beam parameters where the solid line represents the variation predictions. The circle and solid dots represent the corresponding value obtain from the numerical stationary solution and Gaussian feeding, respectively.

as compared to the linear chirp owing to the fact that the Gaussian *ansatz* is a close solution for parabolic graded system [58], and its shape remains almost conserved during propagation. In the case of quadratic waveguide chirping, the beam follows a periodic oscillation reminiscent of the well established self-imaging behavior of Gaussian beam in a continuous parabolic graded index fiber [59]. By considering the contribution of the effective parabolic potential to be more significant than the other two terms, we can simplify the expressions in Eq. (21) and obtain the evolution of the width and phase curvature as $d_\xi n_w = 4n_w \theta$ and $d_\xi \theta = -2\alpha - 4\theta^2 + 1/n_w^4$. This allows us to obtain the expression of the evolution of beam-width n_w in the form of a second order differential equation as

$$d_\xi^2 n_w + 8\alpha n_w - \frac{4}{n_w^3} = 0. \quad (23)$$

This expression is analogous to the evolution of a Gaussian beam width (w) in a continuous graded index medium which is given as $d^2 w/dz^2 + b^2 w - 1/k^2 w^3 = 0$, where b is the index gradient and k is the wavenumber constant [60]. Drawing an analogy

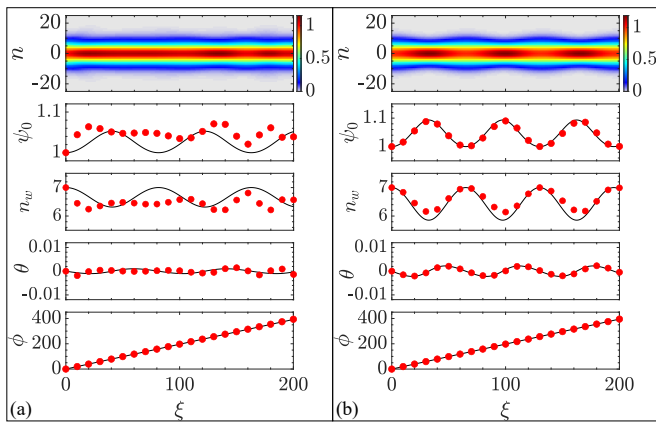


FIG. 6. Evolution of a Gaussian beam with arbitrary width $n_w = 7 (\neq n_{sol})$ in (a) linear (with $\delta = 10$ nm and $\alpha_l = 3 \times 10^{-3}$), and (b) quadratic chirped (with $\delta = 1$ nm, and $\alpha_q = 3 \times 10^{-4}$) WA along with the evolution of the parameters. Solid red dots denotes the numerical data where predictions from the variational analysis are represented by solid black lines.

between these two expressions by making $b = 2\sqrt{2\alpha_q}$ and $k = 1/2$, the evolution of the beam width inside the quadratically chirped WA (with $\alpha_q = 3 \times 10^{-4}$) turns out to be $n_w(\xi) = n_w(0)\sqrt{f(\xi)}$, where $f(\xi) = \cos^2(2\pi\xi/L_p) + C_f^2 \sin^2(2\pi\xi/L_p)$, with $L_p = \pi/\sqrt{2\alpha_q}$, $C_f = (n_{sol}/n_w(0))^2$ and $n_{sol} = 1/\sqrt{kb} = (1/2\alpha_q)^{1/4}$. This expression allows us to determine the self-imaging period where the beam inside the WA is restored to its original width after propagating for a distance of $\xi = L_p/2 \approx 65$. This value corroborates well with the numerical results shown in Figure 6 (b). Inside a WA, a discrete Gaussian beam of arbitrary width can therefore be focused at a distance of $L_p/4$ and this length can be manipulated by the chirping strength.

B. Nonlinear Case (in presence of Kerr nonlinearity)

For high beam powers, when the wave is propagating inside a WA, we can not neglect the nonlinear phenomena emerging through Kerr-effect. The nonlinear Kerr effect leads to the SPM resulting in the self-focusing of the beam. Such self confinement counter balances the beam spreading due to discrete diffraction and eventually an environment is set for a discrete soliton to emerge. [42, 44]. In a uniform WA, where the beam dynamics is described by the normalized DNLS (see Eq. (3)), this balance is achieved with $\mathcal{N} = 1$ for a typical sech-type solution as already shown in Eq. (4).

1. Evolution dynamics of a Gaussian beam in a nonlinear quadratic chirped WA

In this section we focus to explore the role of nonlinearity on a Gaussian beam which is a natural choice for the *ansatz* function in a linear WA. The governing equation of a beam propagating inside a nonlinear quadratic chirped WA is derived in Eq. (9). We adopt the VA for the Gaussian *ansatz* (as given in Eq. (13)) that results in the set of ODE as,

$$d_\xi \psi_0 = (3\alpha n_w^2 - 2) \psi_0 \theta \quad (24a)$$

$$d_\xi n_w = - (3\alpha n_w^2 - 2) 2n_w \theta \quad (24b)$$

$$d_\xi \theta = (3\alpha n_w^2 - 1) 4\theta^2 + \frac{1}{n_w^4} - 2\alpha - \frac{\mathcal{N}^2}{2\sqrt{2}} \frac{\psi_0^2}{n_w^2} \quad (24c)$$

$$d_\xi \phi = 2 - \frac{1}{n_w^2} + \frac{3\alpha}{4} - 3\alpha n_w^4 \theta^2 + \frac{5\mathcal{N}^2}{4\sqrt{2}} \psi_0^2 \quad (24d)$$

Exploiting the set in Eq. (24) we intend to examine the dynamics of a Gaussian beam inside quadratic a chirped WA where Kerr nonlinearity should play a crucial role. In Figure 7(a) we illustrate the beam oscillation owing to the SPM induced self-focusing for a moderate power level of $P_0 = 270$ W (which makes $\mathcal{N} = 0.2$). The variational results (solid red dots) are found to be in well agreement with full numerical results (solid black line). Note that this oscillatory beam dynamics bears a resemblance to the self-focusing observed in parabolic graded index fibers [59, 61]. The evolution of the beam-width is approximately governed by the following ordinary second order differential equation,

$$d_\xi^2 n_w + 8\alpha_q n_w - \frac{4}{n_w^3} - \sqrt{\frac{2}{\pi}} \mathcal{N}^2 E \frac{1}{n_w^2} = 0 \quad (25)$$

where $E = \int_{-\infty}^{\infty} |\psi|^2 dn = \sqrt{\pi} \psi_0(0)^2 n_w(0)$ is the total energy which is conserved. The ODE as shown in Eq. (25) predicts nicely the oscillatory nature of Gaussian beam for moderate nonlinearity (with $\mathcal{N} \leq 0.5$). The analytical results (solid black lines) are found to be in decent agreement with full numerical simulation (red dashed line) as shown in Figure 7(b). Gradual increment of power results in a strong beam compression. When the beam is compressed to almost a point it merely encompasses two or three waveguides and no longer be in a Gaussian shape. Note, under such situation the continuous approximation we considered in deriving Eq. (6) is also violated. Such strong confinement causes the formation of Peierls-Nabarro (PN) potential barrier for localized modes in nonlinear lattices [3]. This PN potential eventually leads to the formation of a stop-band in the nonlinear WA for fields with strong amplitude and narrow widths [62, 63] and restricts any transverse motion. A similar scenario is manifested in Figure 7 (c) where a strong nonlinearity ($\mathcal{N} = 0.8$) leads to a strong beam confinement that is eventually limited to the central waveguide. The

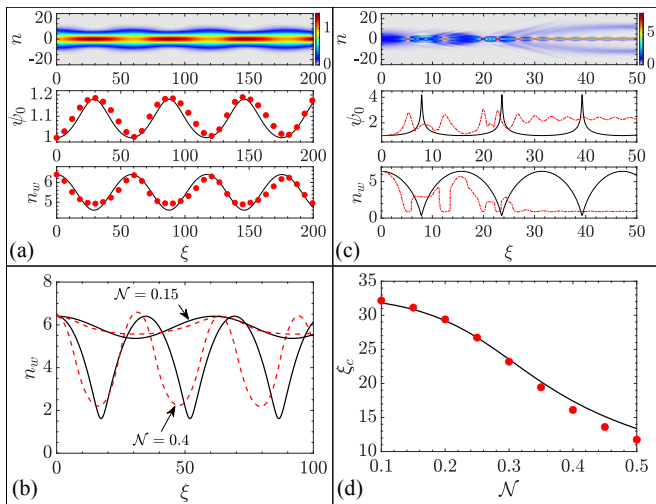


FIG. 7. Evolution of a Gaussian beam under the influence of nonlinear Kerr effect for (a) $\mathcal{N} = 0.2$ and (c) $\mathcal{N} = 0.8$. In the inset we demonstrate how amplitude (ψ_0) and beam-width (n_w) are affected by SPM. For relatively low power level ($\mathcal{N} = 0.2$) at which the distortion of the Gaussian beam shape is tolerable, variational analysis (solid lines) agrees well with numerical data (solid dots). In plot (b) we portray the variation of oscillatory beam-width for two different \mathcal{N} values where variational analysis (solid lines) are corresponding numerical data (dotted lines) are compared. In plot (d) we show how the oscillation period (ξ_c) decreases with increasing nonlinearity (\mathcal{N}) and the variational prediction (solid line) is consistent with full numerical analysis (solid dots).

strong confinement of the optical beam, owing to large nonlinearity, incurs a significant distortion in the Gaussian beam shape, resulting in a mismatch between variational results and full numerical data as illustrated in Figure 7 (c). We examine the oscillatory beam dynamics for various \mathcal{N} and find that the oscillation period (ξ_c) reduces with increasing \mathcal{N} . We demonstrate this variation in Figure 7 (d), where our analytical prediction (black solid line) matches well with numerical results (solid red dots). While in the absence of nonlinearity ($\mathcal{N} = 0$) in a quadratic chirped WA, the stationary solution is obtained in the form of a Gaussian beam, the same cannot be said for $\mathcal{N} \neq 0$. In other words, a Gaussian beam is not a natural solution (or steady state solution) under nonlinearity, rather it collapses at high nonlinearity. Next we seek for a stationary solution having the form $a_n(\xi) = u(n)e^{-i\beta\xi}$, and incorporating it in the DNSLE we get,

$$-\beta u(n) + \eta_n^{n+1} u(n+1) + \eta_{n-1}^n u(n-1) + \mathcal{N}^2 u(n)^3 = 0. \quad (26)$$

For a quadratic chirped WA, we numerically solve Eq. (26) for different \mathcal{N} values. In Figure 8 (a), we compare the numerically obtained steady-state solutions with the Gaussian and sech-type *ansatz* function that we consider in our study. The figure shows that, with increasing non-

linearity (\mathcal{N}), the shape of the stationary solution is gradually squeezed in n -space (transverse coordinate) and eventually takes a form $\text{sech}(n/\sqrt{2})$ which represents a soliton solution (see Eq. (4)). Hence in the limit $\mathcal{N} \rightarrow 1$, being a natural solution, the sech-type beam apparently much more stable compared to a Gaussian beam. Because of this reason, now we consider the sech-type beam as our *ansatz* for VA and investigate its dynamics in the chirped WA.

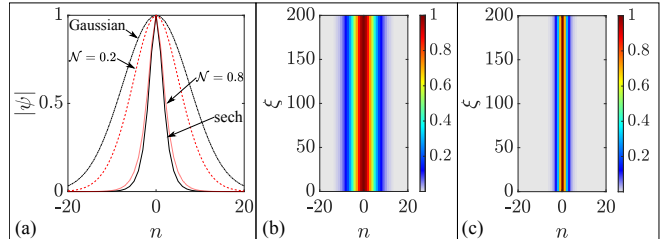


FIG. 8. (a) We compare the full numerical solution with Gaussian solution (dashed dotted) as per Eq. (22) for low nonlinearity ($\mathcal{N} = 0.2$) and for high nonlinearity ($\mathcal{N} = 0.8$) with sech-type shape which is a natural solution in a uniform WA. Evolution of the stationary solution for (b) $\mathcal{N} = 0.2$ (dashed line in (a)) and (c) $\mathcal{N} = 0.8$ (dotted line in (a)) under a chirping strength of $\delta = 1\text{nm}$.

C. Linear stability analysis of the stationary solutions

In the previous section we numerically obtain the stationary solution inside the linear and quadratic chirped WA in absence of Kerr nonlinearity. To check the stability of the numerically obtained solutions we may proceed with the linear stability analysis (LSA). We perturbed the stationary solution with a small amplitude,

$$a_n(\xi) = \left[u_n + v_n e^{-i\lambda\xi} + w_n^* e^{i\lambda^*\xi} \right] e^{i\beta\xi}, \quad (27)$$

where, v_n and w_n are small amplitude complex perturbations to the stationary solution u_n , with complex propagation constants λ [64]. The substitution of this field into the governing DNLSE (see Eq. (2)), and respective linearization of v_n and w_n (as $v_n, w_n \ll u_n$), leads to the eigenvalue problem

$$\mathcal{M}X = \lambda X \quad (28)$$

where $X = \begin{bmatrix} V \\ W \end{bmatrix}$ with $V = [v_{-N}; v_{-N+1}; \dots; v_0; \dots; v_{(N-1)}; v_N]$, $W = [w_{-N}; w_{-N+1}; \dots; w_0; \dots; w_{(N-1)}; w_N]$ and \mathcal{M} is a

$2(2N + 1) \times 2(2N + 1)$ matrix given as

$$\mathcal{M} = \begin{bmatrix} D_{-N} & -\eta_{-N}^{-N+1} & 0 & \cdot & \cdot & \cdot & \cdot & \cdot & \cdot & 0 \\ \cdot & \cdot \\ \cdot & -\eta_{n-1}^n & D_n & -\eta_n^{n+1} & \cdot & \cdot & \cdot & \cdot & \cdot & \cdot \\ \cdot & \cdot \\ \cdot & \cdot & -\eta_{N-1}^N & D_N & 0 & 0 & \cdot & \cdot & \cdot & \cdot \\ \cdot & \cdot & \cdot & \cdot & \cdot & G_{-N} & \eta_{-N}^{-N+1} & \cdot & \cdot & \cdot \\ \cdot & \cdot \\ \cdot & \cdot \\ \cdot & \cdot & \cdot & \cdot & \cdot & \cdot & \eta_{n-1}^n & G_n & \eta_n^{n+1} & \cdot \\ \cdot & \cdot \\ 0 & \cdot & \cdot & \cdot & \cdot & \cdot & 0 & 0 & \eta_{N-1}^N & G_N \end{bmatrix} \quad (29)$$

where $D_n = \beta - \mathcal{N}^2 (2|u_n|^2 + u_n^{*2})$, $G_n = -\beta + \mathcal{N}^2 (2|u_n|^2 + u_n^{*2})$, and $(2N + 1)$ is the total number of waveguides. The off-diagonal elements of the matrix \mathcal{M} corresponds to the coupling coefficients and are determined by the corresponding chirping scheme of the system, while the diagonal terms are derived from the propagation constant (β) and self phase modulation ($\mathcal{N}^2(2|u|^2 + u_n^{*2})$) terms of the stationary solution u_n . The matrix form reduces the determination of the localized solutions of v_n and w_n in to a eigenvalue problem with $\lambda = \text{Eig}(\mathcal{M})$. Eigenvalues with $\text{Im}(\lambda) \neq 0$ indicate the instability growth where the perturbation grows with propagation as v_n or w_n increase exponentially and the stationary solution is unstable.

We perform the LSA for the solutions obtained numerically in case of linear and quadratic chirped WA in presence and absence of Kerr nonlinearity. In Figure 9 we summarize the LSA for all four cases. Note, the eigen values obtained for all four cases are found to be absolutely real implying the fact that the solutions are stable under the effects of perturbations [64]. We numerically check this stability by solving the DNLSE with an input (that we find numerically) corrupted with noise having 10% of peak solution amplitude. As demonstrated in Figure 9, the numerical simulation shows stability as predicted by LSA. We further emphasize, that the two discrete points in the eigenvalue spectra depicted in Figure 9 (d) should correspond to oscillating modes [65] and the same can be observed in the numerical results.

D. Dynamics of discrete soliton in chirped WA

In the previous sections it is already established that a Gaussian beam is not the stationary solution of Eq. (3) for a nonlinear WA. Rather, a sech-type beam, in the form of discrete soliton, is found to be the exact solution under Kerr effect. Hence we employ sech-type shape as our *ansatz* for VA. Note, the accuracy of the results based on VA is sensitive to the choice of *ansatz* function. VA relies on the assumption that the shape of the *ansatz*

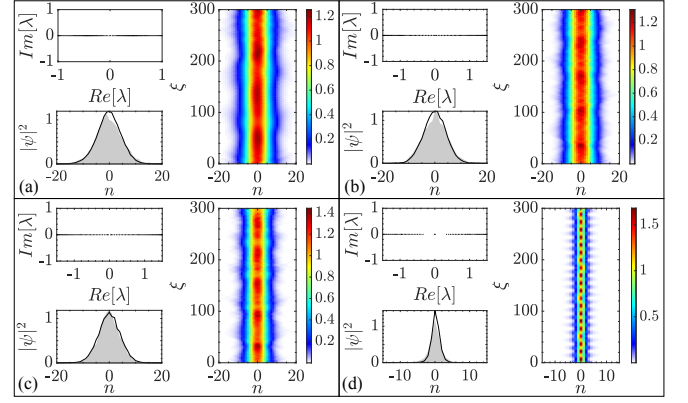


FIG. 9. Evolution of numerical solution in the absence of Kerr self-focusing, obtained under (a) linear and (b) quadratic chirping for $\mathcal{N} = 0$, and for (c) $\mathcal{N} = 0.2$ and (d) $\mathcal{N} = 0.8$ under quadratic chirping with a random noise with an amplitude of 10% of the peak solution amplitude. The growth parameter $\text{Im}(\lambda)$ is found to be zero for all the cases confirming the stability of the solution. The insets also demonstrate the superposition of the input and output beam showing marginal distortion under input noise.

function should not vary over propagation under perturbation. The governing equation for a quadratic chirped WA system can be written as,

$$i\partial_\xi \psi + 2\psi + \partial_n^2 \psi + |\psi|^2 \psi = i\epsilon, \quad (30)$$

where ϵ accounts for the perturbation owing to waveguide chirping. The corresponding Lagrangian density \mathcal{L} for Eq. (30) is constructed as,

$$\mathcal{L} = \frac{i}{2} (\psi \partial_\xi \psi^* - \psi^* \partial_\xi \psi) - 2|\psi|^2 + |\partial_n \psi|^2 - \frac{1}{2} |\psi|^4 + i(\epsilon \psi^* - \epsilon^* \psi). \quad (31)$$

As an *ansatz*, we consider the generalized soliton solution by incorporating the transverse wavenumber κ_0 as [46],

$$\psi(n, \xi) = \psi_0 \text{sech} \left[\frac{\psi_0(n - n_0)}{\mathcal{D}} \right] e^{i\phi + i\kappa_0(n - n_0)}, \quad (32)$$

where ψ_0 , n_0 , κ_0 , and ϕ are the soliton parameters representing amplitude, peak position, central wavenumber, and phase respectively, and $\mathcal{D} = \sqrt{2 \cos(\kappa_0(0))}$. We reduce the Lagrangian by adopting the *ansatz* function as $L = \int_{-\infty}^{\infty} \mathcal{L} dn$, and get

$$L = \left(d_\xi \phi - \kappa d_\xi n_0 + \kappa^2 - 2 \right) 2\mathcal{D}\psi_0 + \frac{2}{3} \left(\frac{1}{\mathcal{D}} - \mathcal{D} \right) + \int_{-\infty}^{\infty} i(\epsilon \psi^* - \epsilon^* \psi) dn \quad (33)$$

Employing the *Euler-Lagrangian equation* [57] we finally obtain the following set of ODE showing how the beam parameters are affected due to chirping in the arrange-

ment of a WA.

$$d_\xi \psi_0 = \frac{1}{2\mathcal{D}} P_\phi \quad (34a)$$

$$d_\xi \kappa_0 = -\frac{1}{2\mathcal{D}\psi_0} (\kappa_0 P_\phi + P_{n_0}) \quad (34b)$$

$$d_\xi n_0 = 2\kappa_0 + \frac{1}{2\mathcal{D}\psi_0} P_{\kappa_0} \quad (34c)$$

$$d_\xi \phi = 2 + \psi_0^2 + \kappa_0^2 - \frac{\psi_0^2}{\mathcal{D}^2} + \frac{1}{2\mathcal{D}\psi_0} (\kappa_0 P_{\kappa_0} - \psi_0 P_{\psi_0}). \quad (34d)$$

Here, P_ν are defined as $P_\nu = \int_{-\infty}^{\infty} i(\epsilon \partial_\nu \psi^* - \epsilon^* \partial_\nu \psi) dn$, which can be evaluated separately for each parameter ν under the appropriate perturbation ϵ .

1. Linear Chirping

In case of linearly chirped WA, where the propagating beam dynamics is governed by Eq. (8) the perturbation term due to chirping is given by,

$$\epsilon_l = -i\alpha_l \left(|n| 2\psi + |n| \partial_n^2 \psi + \text{sgn}(n) \partial_n \psi \right). \quad (35)$$

For this given ϵ_l , P_ν are obtained as,

$$P_\phi = 0 \quad (36a)$$

$$P_{n_0} = -\frac{2\alpha_l \mathcal{D}^2}{3} \mathcal{A} \chi_t \left[\mathcal{A}^2 \chi_t^2 + 3\mathcal{B} \right] \quad (36b)$$

$$P_{\kappa_0} = 4\alpha_l \mathcal{D}^2 \kappa_0 \log \left[\frac{\chi_s}{2} \right] \quad (36c)$$

$$P_{\psi_0} = -\left[\frac{1}{3} \mathcal{A}^2 \chi_t^2 + \mathcal{B} \right] 2\alpha \mathcal{D} n_0 \chi_t - \frac{4\alpha_l \psi_0}{3} \left[\frac{\chi_s^2}{2} + \log(2/\chi_s) \right] \quad (36d)$$

where $\mathcal{A} = \psi_0/\mathcal{D}$, and $\mathcal{B} = (\kappa_0^2 - 2)$, with $\chi_t = \tanh(\mathcal{A}n_0)$ and $\chi_s = \text{sech}(\mathcal{A}n_0)$. Note, one can obtain the equation of motion for the different beam parameters under linear chirping by plugging Eq. (36) in Eq. (34). For a chirping strength of $\delta = 2.5$ nm, in Figure 10 (a)-(d), we plot the beam dynamics and the evolution of different beam parameters. We compare the results predicted from the VA and the CME for three different sets of initial conditions (i) $n_0 = 0$ and $\kappa_0 = 0$, (ii) $n_0 = 10$ and $\kappa_0 = 0$, and (iii) $n_0 = 0$ and $\kappa_0 = 0.1$. In Figure 10 (a) and (c) we illustrate the beam dynamics in n and κ space, respectively. The variational predictions (white dashed lines) shown in Eq. (36) are superimposed on the mesh plot obtained numerically by directly solving the DNLSE given in Eq. (2). The oscillatory dynamics of the propagating beam is accurately predicted by the variational results under different initial conditions where the beam is launched at different waveguide channel (n_0)

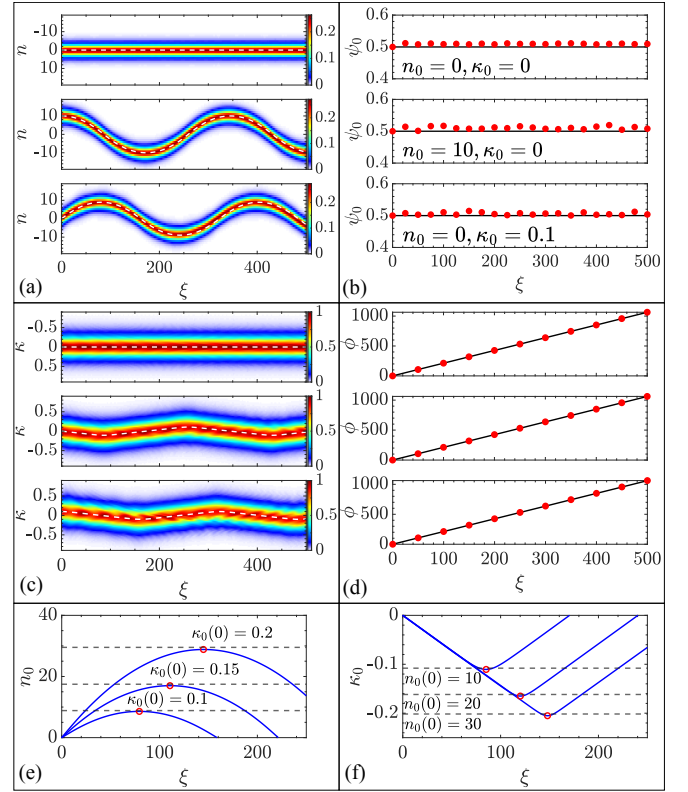


FIG. 10. Evolution of a DS under linear chirp for three initial cases (i) $n_0(0) = 0$ and $\kappa_0(0) = 0$, (ii) $n_0(0) = 10$ and $\kappa_0(0) = 0$, and (iii) $n_0(0) = 0$ and $\kappa_0(0) = 0.1$ for chirping strength of $\delta = 2.5$ nm. The evolution of the soliton in the (a) n -space and (c) κ -space is shown for each case with the prediction of the central location from the variational analysis given by dashed white lines. The corresponding evolution of the (b) amplitude and (d) phase as per the DNLSE (solid red circles) and variational analysis (solid lines), respectively. Plot (e) and (f) shows the trace of beam position in n and κ space for different $n_0(0)$ and $\kappa_0(0)$ values. The beam location limit (red dots on the curve) agrees well with analytical prediction (horizontal dotted lines).

and transverse wavenumber (κ_0). The amplitude (ψ_0) and phase (ϕ) variations for such condition are also captured in Figure 10 (b) and (d) where VA shows a decent agreement with numerical results. We note that, the contributions of the terms involving derivatives ($-i\alpha_l |n| \partial_n^2 \psi$ and $-i \text{sgn}(n) \alpha_l \partial_n \psi$) in ϵ_l , are marginal and hence can be neglected for low chirping strength. Employing this assumption we obtain relatively simpler expressions for beam position and wavenumber dynamics as,

$$d_\xi n_0 = 2\kappa_0 \quad (37a)$$

$$d_\xi \kappa_0 = -2\alpha_l \tanh(\mathcal{A}n_0), \quad (37b)$$

which leads to the compact equation predicting the peak location of oscillatory beam as, $d_\xi^2 n_0 = -4\alpha_l \tanh(\mathcal{A}n_0)$. The closed form solution of this differential equation is found to be elusive. However, the set of equation Eq. (37) allow us to obtain few important information re-

garding the beam dynamics. For example, when the input beam is launched normally away from the central waveguide ($n_0(0) \neq 0, \kappa_0(0) = 0$) the transverse wavenumber evolves till it reaches a maximum value $\kappa_{max} = \sqrt{\frac{2\alpha_l}{\mathcal{A}} \log \left(\cosh [\mathcal{A}n_0(0)] \right)}$. In another launching scheme where the beam is launched at the central waveguide with an angle ($n_0(0) = 0, \kappa_0(0) \neq 0$), we observe the beam travels within a limiting waveguide channel defined as, $n_{max} = \frac{1}{\mathcal{A}} \cosh^{-1} \left[\exp \left(\frac{\mathcal{A}\kappa_0^2(0)}{2\alpha_l} \right) \right]$. Note that, in the limit $n_0(0) \rightarrow 0$ and $\kappa_0(0) \rightarrow 0$, $k_{max} = 0$ and $n_{max} = 0$, that means under normal launching to central waveguide the beam propagates straight without exhibiting any oscillatory dynamics. This result is in agreement with full numerical simulation. In Figure 10 (e) and (f) we trace the beam position over propagation distance in n and κ space for different launching angles ($\kappa_0(0)$) and sites ($n_0(0)$). As depicted in plot (e), in all the cases maxima of the beam location from central waveguide (red dots on the curve) agrees well with analytical predictions represented as horizontal dotted lines. In case of off-shifted ($n_0 \neq 0$) normal launching ($\kappa_0(0) = 0$), as demonstrated in plot (f) the transverse wavevector κ_0 reaches to a maxima (red dots on the curve) and revert back where the numerical results are in agreement with analytical predictions.

2. Quadratic Chirping

Next we extend our investigation inside a quadratic chirped WA for which the propagating beam is governed by the effective NLSE derived in Eq. (9). For this WA, the chirp induced perturbation can be quantified as,

$$\epsilon_q = -i\alpha_q \left(2n^2\psi - n^2\partial_n^2\psi - 2n\partial_n\psi \right). \quad (38)$$

Implementing ϵ_q in the NLSE Eq. (30) we derive P_ν ,

$$P_\phi = 0 \quad (39a)$$

$$P_{\kappa_0} = -4\alpha_q \mathcal{D}\psi_0 \left(n_0^2 + \frac{\pi^2}{12} \frac{1}{\mathcal{A}^2} \right) \quad (39b)$$

$$P_{n_0} = -4\alpha_q \mathcal{D}\psi_0 n_0 \left(\frac{\mathcal{A}^2}{3} + \mathcal{B} \right) \quad (39c)$$

$$P_{\psi_0} = 2\alpha_q \mathcal{D} \left[\frac{\pi^2}{12} \left(\frac{\mathcal{B}}{\mathcal{A}^2} - \frac{1}{3} \right) + (\mathcal{A}^2 - \mathcal{B}) n_0^2 - \frac{1}{3} \right]. \quad (39d)$$

Now plugging Eq. (39), in Eq. (34) one can get the equation of motion for different beam parameters under quadratic chirping. For a chirping strength of $\delta = 0.25$ nm, the comparison between the variational results, and the CME is illustrated in Figure 11 for three different initial conditions (i) $n_0 = 0$ and $\kappa_0 = 0$, (ii) $n_0 = 10$ and $\kappa_0 = 0$, and (iii) $n_0 = 0$ and $\kappa_0 = 0.1$. The vari-

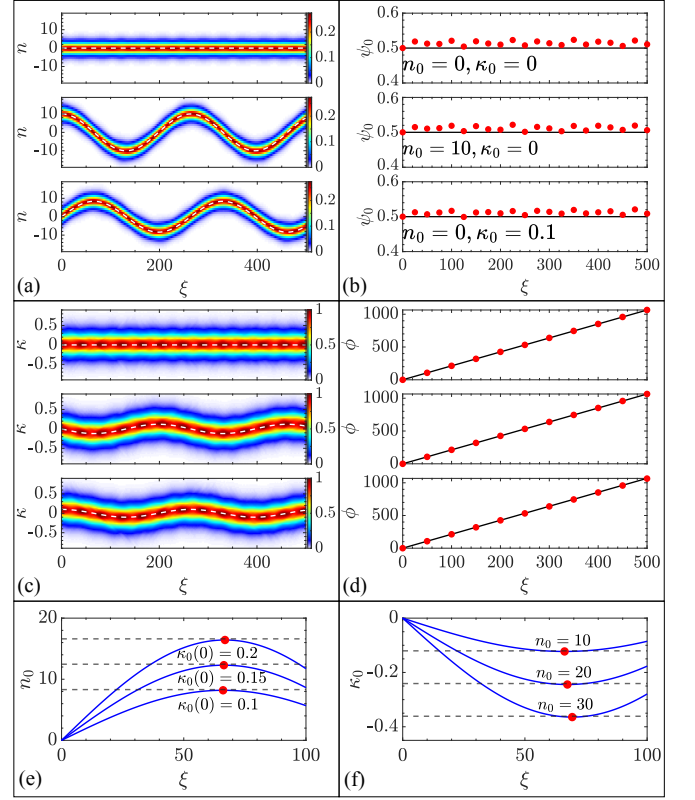


FIG. 11. Evolution of a DS under quadratic chirp for three initial cases (i) $n_0(0) = 0$ and $\kappa_0(0) = 0$, (ii) $n_0(0) = 10$ and $\kappa_0(0) = 0$, and (iii) $n_0(0) = 0$ and $\kappa_0(0) = 0.1$ for chirping strength of $\delta = 0.25$ nm. The evolution of the soliton in the (a) n -space and (c) κ -space is shown for each case with the prediction of the central location from the variational analysis is given by dashed white lines. The corresponding evolution of the (b) amplitude and (d) phase as per the DNLSE (solid red circles) and variational analysis (solid lines), respectively. Plot (e) and (f) shows the trace of beam position in n and κ space for different $n_0(0)$ and $\kappa_0(0)$ values. The beam location limit (red dots on the curve) agrees well with analytical prediction (horizontal dotted lines).

ational results (white dashed lines) accurately trace the beam location in n (plot Figure 11 (b)) and κ (Figure 11 (c)) space, respectively. Further we demonstrate the evolution of ψ_0 and ϕ in Figure 11 (b) and (d). Eq. (34d) is further simplified by neglecting the last two terms in ϵ_q whose contribution is found to be negligible and we get a compact set of ODE as,

$$d_\xi n_0 = 2\kappa_0 \quad (40a)$$

$$d_\xi \kappa_0 = -4\alpha_q n_0. \quad (40b)$$

Combining Eq. (40b) we can get the standalone expression for n_0 as $d_\xi^2 n_0 = -8\alpha_q n_0$ that describes the oscillatory motion of the soliton under the quadratic potential with a period $\xi_c \approx \pi/\sqrt{2\alpha_q}$. When the central waveguide is illuminated at an angle, the position (n_0) and transverse wavevector (κ_0) of the beam evolve as, $n_0(\xi) = n_{max} \sin(2\sqrt{2\alpha_q}\xi)$ and $\kappa_0(\xi) = \kappa_0(0) \cos(2\sqrt{2\alpha_q}\xi)$, with

$n_{max} = \kappa_0(0)/\sqrt{2\alpha_q}$. For the other case, when a soliton is launched normally and shifted from the central waveguide ($\kappa_0(0) = 0$, $n_0(0) \neq 0$), it evolves as $n_0(\xi) = n_0(0) \cos(2\sqrt{\alpha_q}\xi)$ and $\kappa_0(\xi) = \kappa_{max} \sin(2\sqrt{2\alpha_q}\xi)$, with $\kappa_{max} = -\sqrt{2\alpha_q}n_0(0)$. In Figure 11 (a)-(d) we depict the beam evolution in n and κ space with the variation of its amplitude and phase. The unique oscillatory nature guided by the symmetric chirping of the waveguide arrangement is nicely predicted in analytical results that corroborate well with numerical calculations. For the chirping strength $\delta = 0.25$ nm ($\alpha_q = 7.25 \times 10^{-5}$) we numerically obtain $\xi_c \approx 260$ which is very close to our analytical prediction. In Figure 11 (e)-(f) we numerically trace the beam path (blue solid line) in n and κ space for different launching angles $\kappa_0(0)$ (see plot (e)) and sites $n_0(0)$ (see plot (f)). The terminal point of the paths are indicated by red solid dots which agrees well with our analytical predictions represented by horizontal dotted lines.

In summary, for both chirping schemes, we demonstrate that the solitons evolve in a sinusoidal path in n -space where the evolution of the transverse wavenumber κ_0 exhibits an unique zig-zag (linear chirping) or a sinusoidal (quadratic chirping) variation. The dynamics of the soliton beam are accurately captured by the proposed VA for both the chirping schemes. Based on the analytic results, we further derive the expressions for the maximum displacement of solitons in n and κ space that matches well with full numerical simulation.

IV. CONCLUSION

Waveguide array offers a compact and stable platform in structuring the light for versatile applications ranging from solid state to quantum physics. In this article we aim to investigate the dynamics of beam evolution inside specifically engineered waveguide arrays. We propose two types of symmetrically chirped waveguide arrangement where the separation between consecutive waveguide channels either changes linearly or in quadratic fashion. The non-uniformity of the waveguide separation makes the coupling coefficient between two adjacent waveguide channel a function of transverse coordinate which we derive by adopting a continuous approximation. Such approximation is justified due the fact that the propagating beam encompasses many waveguides and in fact allows us to derive the continuous counterpart of the DNLSE. The effect of chirping is accounted by expressing the coupling coefficient as a continuous function of the transverse coordinate. Assuming the chirping strength to be small we further simplify the expression of coupling coefficient and derive a modified DNLSE that should capture the beam dynamics in the chirped waveguide array. To justify the correctness of our derived equations we compare it with the original DNLSE and demonstrate that both equations produce identical results. The continuous counterpart of the original DNLSE facilitates us

to utilize the semi-analytical variational technique that unfold the complex dynamics of the beam propagation in a chirped system by producing a set of ordinary differential equations of the different beam parameters. Exploiting the variational results we predict several interesting features of the beam dynamics. For example, we noticed that, a chirped waveguide array mimics a graded index media where the transversely varying coupling coefficient plays a role identical to that of the refractive index in the graded system. We establish identical results in the context of beam dynamics for these two separate systems. We demonstrate that for a linear case (without Kerr nonlinearity) a steady state solution can be obtained in the proposed chirped waveguide array and determine the initial condition to get such solution by exploiting the variational results where we adopt a Gaussian beam as an ansatz (or trial function). When the input parameters (amplitude or width) of the Gaussian beam are away from the steady state condition we observe an oscillatory propagation well supported by the variational prediction. Under nonlinearity, however, the Gaussian beam oscillates and does not produce any steady state solution because it is not an exact solution. The variational results whose accuracy relies on the correct choice of ansatz also deviate from the numerical analysis in this regime. However, numerically it is possible to obtain a stationary solutions for such systems. First we obtain the steady solution and also perform a linear stability analysis to examine its robustness. The formation of discrete soliton is inevitable under nonlinearity and finally we exploit such a solution in sech-form when discrete diffraction is counterbalanced by the system nonlinearity. We investigate the dynamics of such stable soliton inside the chirped waveguide array under different input conditions. The waveguide chirping behaves as a perturbation and we obtain unique oscillatory dynamics for such systems that corroborate well with analytical predictions.

In conclusion, with the current requirements of on-chip level control and routing of beams and signals, optical lattices, that adds extra degrees of freedom to modulate the light dynamics such as chirped WAs, may be a potential platform for structuring light. In this work we model such a versatile waveguide structure and provide a detailed and comprehensive study on the beam dynamics in linear and non-linear domain. Several interesting features are revealed in the context of beam propagation that may be useful for future applications.

ACKNOWLEDGMENTS

A.P.L. and S.R. are grateful to Anusandhan National Research Foundation (ANRF), erstwhile SERB, India, for providing financial support to carry out this work under the CRG program.

Appendix A: Derivation of the approximated continuous form of DNSE

1. Linear Chirping

Considering the coupling profile for the symmetric linear chirping as $\eta_n^{n+1} \approx e^{-\alpha|n+\frac{1}{2}|}$, we can evaluate the term $\eta_n^{n+1} \pm \eta_{n-1}^n$ present in Eq. (7). To proceed with this evaluation we have to consider the two domains of n , i.e $n \geq 0$ and $n < 0$, where $\eta_n^{n+1} = \exp[-\alpha_l(n+1/2)]$ for $n \geq 1$, and $\eta_n^{n+1} = \exp[\alpha_l(n+1/2)]$.

$$\eta_n^{n+1} \pm \eta_{n-1}^n = \begin{cases} e^{-\alpha_l n} \left(e^{-\alpha_l/2} \pm e^{\alpha_l/2} \right) & n \geq 0 \\ e^{\alpha_l n} \left(e^{\alpha_l/2} \pm e^{-\alpha_l/2} \right) & n < 0 \end{cases} \quad (\text{A1})$$

Exploiting the identities $2 \cosh(x) = e^x + e^{-x}$ and $2 \sinh(x) = e^x - e^{-x}$, we can write Eq. (7) in the two regimes as,

$$\begin{aligned} i\partial_\xi \psi + \mathcal{N}^2 |\psi|^2 \psi + 2 \cosh\left(\frac{\alpha_l}{2}\right) e^{-\alpha_l n} \left(\psi + \frac{1}{2} \partial_n^2 \psi \right) \\ - 2 \sinh\left(\frac{\alpha_l}{2}\right) e^{-\alpha_l n} \partial_n \psi = 0 \end{aligned} \quad (\text{A2})$$

for $n \geq 0$, and

$$\begin{aligned} i\partial_\xi \psi + \mathcal{N}^2 |\psi|^2 \psi + 2 \cosh\left(\frac{\alpha_l}{2}\right) e^{\alpha_l n} \left(\psi + \frac{1}{2} \partial_n^2 \psi \right) \\ + 2 \sinh\left(\frac{\alpha_l}{2}\right) e^{\alpha_l n} \partial_n \psi = 0 \end{aligned} \quad (\text{A3})$$

for $n < 0$. Using the signum function $\text{sgn}(n)$ for n , the two equations can be written in a single equation as

$$\begin{aligned} i\partial_\xi \psi + \partial_n^2 \psi + 2\psi + \mathcal{N}^2 |\psi|^2 \psi \\ + \left[\cosh\left(\frac{\alpha_l}{2}\right) e^{-\alpha_l |n|} - 1 \right] (2\psi + \partial_n^2 \psi) \\ - 2 \text{sgn}(n) \sinh\left(\frac{\alpha_l}{2}\right) e^{-\alpha_l |n|} \partial_n \psi = 0. \end{aligned} \quad (\text{A4})$$

In this expression, the first four terms are the standard terms of the NLSE, fifth and sixth term correspond the effective potential and variation in diffraction coefficient along the transverse axis due to the changing coupling coefficient. The last term is a transverse velocity imparted to the field due to the asymmetry in the coupling coefficient about the n^{th} waveguide. Applying the Taylor series expansion of $\cosh(\alpha_l/2)$, $\sinh(\alpha_l/2)$, and $\exp(-\alpha_l |n|)$ and neglecting the terms containing higher order of α_l (as $\alpha_l \approx 10^{-3}$) we may write the approximate continuous NLSE as

$$\begin{aligned} i\partial_\xi \psi + \partial_n \psi + 2\psi + \mathcal{N}^2 |\psi|^2 \psi - \alpha_l |n| (2\psi + \partial_n^2 \psi) \\ - \text{sgn}(n) \alpha_l \partial_n \psi = 0 \end{aligned} \quad (\text{A5})$$

2. Quadratic Chirping

In the case of the quadratic chirping the functional form of the coupling coefficient profile is obtained as $\eta_n^{n+1} \approx \exp\left[-\alpha_q \left(n + \frac{1}{2}\right)^2\right]$. With this form, the $\eta_n^{n+1} \pm \eta_{n-1}^n$ terms can be expressed as

$$\eta_n^{n+1} \pm \eta_{n-1}^n = e^{-\alpha_q (n^2+1/4)} (e^{-\alpha_q n} \pm e^{\alpha_q n}). \quad (\text{A6})$$

This modification leads to the continuous approximation of the DNLS as

$$\begin{aligned} i\partial_\xi \psi + 2\psi + \partial_n^2 \psi + \mathcal{N}^2 |\psi|^2 \psi \\ + \left[\cosh(\alpha_q n) e^{-\alpha_q (n^2+1/4)} - 1 \right] (2\psi + \partial_n^2 \psi) \\ - 2 \sinh(\alpha_q n) e^{-\alpha_q (n^2+1/4)} \partial_n \psi = 0. \end{aligned} \quad (\text{A7})$$

Expanding the functions involved in the equation in Taylor series and neglecting the higher order terms of α_q we further simplify the governing equation and obtain the expression as,

$$\begin{aligned} i\partial_\xi \psi + 2\psi + \partial_n^2 \psi + \mathcal{N}^2 |\psi|^2 \psi - \alpha_q n^2 (2\psi + \partial_n^2 \psi) \\ - 2\alpha_q n \partial_n \psi = 0 \end{aligned} \quad (\text{A8})$$

[1] T. Pertsch, P. Dannberg, W. Elflein, A. Bräuer, and F. Lederer, Optical Bloch Oscillations in Temperature Tuned Waveguide Arrays, *Physical Review Letters* **83**,

4752 (1999).

[2] R. Morandotti, U. Peschel, J. S. Aitchison, H. S. Eisenberg, and Y. Silberberg, Experimental Observation of

- Linear and Nonlinear Optical Bloch Oscillations, *Physical Review Letters* **83**, 4756 (1999).
- [3] Y. S. Kivshar and D. K. Campbell, Peierls-Nabarro potential barrier for highly localized nonlinear modes, *Physical Review E* **48**, 3077 (1993).
- [4] Y. Lahini, A. Avidan, F. Pozzi, M. Sorel, R. Morandotti, D. N. Christodoulides, and Y. Silberberg, Anderson Localization and Nonlinearity in One-Dimensional Disordered Photonic Lattices, *Physical Review Letters* **100**, 013906 (2008).
- [5] S. Longhi, Klein tunneling in binary photonic superlattices, *Physical Review B* **81**, 075102 (2010).
- [6] F. Dreisow, M. Heinrich, R. Keil, A. Tünnermann, S. Nolte, S. Longhi, and A. Szameit, Classical Simulation of Relativistic *Zitterbewegung* in Photonic Lattices, *Physical Review Letters* **105**, 143902 (2010).
- [7] S. Longhi, Photonic analog of zitterbewegung in binary waveguide arrays, *Optics Letters* **35**, 235 (2010).
- [8] A. Marini, S. Longhi, and F. Biancalana, Optical Simulation of Neutrino Oscillations in Binary Waveguide Arrays, *Physical Review Letters* **113**, 150401 (2014).
- [9] A. Marini, T. X. Tran, S. Roy, S. Longhi, and F. Biancalana, Optical analog of spontaneous symmetry breaking induced by tachyon condensation in amplifying plasmonic arrays, *Physical Review A* **89**, 023840 (2014).
- [10] A. Perez-Leija, H. Moya-Cessa, A. Szameit, and D. N. Christodoulides, Glauber–Fock photonic lattices, *Optics Letters* **35**, 2409 (2010).
- [11] R. Keil, A. Perez-Leija, F. Dreisow, M. Heinrich, H. Moya-Cessa, S. Nolte, D. N. Christodoulides, and A. Szameit, Classical Analogue of Displaced Fock States and Quantum Correlations in Glauber-Fock Photonic Lattices, *Physical Review Letters* **107**, 103601 (2011).
- [12] T. X. Tran, X. N. Nguyen, and F. Biancalana, Dirac solitons in square binary waveguide lattices, *Physical Review A* **91**, 023814 (2015).
- [13] D. Mihalache, D. Mazilu, F. Lederer, and Y. S. Kivshar, Spatiotemporal dissipative solitons in two-dimensional photonic lattices, *Physical Review E* **78**, 056602 (2008).
- [14] S. Minardi, F. Eilenberger, Y. V. Kartashov, A. Szameit, U. Röpke, J. Kobelke, K. Schuster, H. Bartelt, S. Nolte, L. Torner, F. Lederer, A. Tünnermann, and T. Pertsch, Three-Dimensional Light Bullets in Arrays of Waveguides, *Physical Review Letters* **105**, 263901 (2010).
- [15] P. S. Vinayagam, A. Javed, and U. A. Khawaja, Stable discrete soliton molecules in two-dimensional waveguide arrays, *Physical Review A* **98**, 063839 (2018).
- [16] S. Suntsov, K. G. Makris, D. N. Christodoulides, G. I. Stegeman, A. Haché, R. Morandotti, H. Yang, G. Salamo, and M. Sorel, Observation of Discrete Surface Solitons, *Physical Review Letters* **96**, 063901 (2006).
- [17] L. Dong, Y. V. Kartashov, L. Torner, and A. Ferrando, Vortex Solitons in Twisted Circular Waveguide Arrays, *Physical Review Letters* **129**, 123903 (2022).
- [18] C. R. Rosberg, I. L. Garanovich, A. A. Sukhorukov, D. N. Neshev, W. Krolikowski, and Y. S. Kivshar, Demonstration of all-optical beam steering in modulated photonic lattices, *Optics Letters* **31**, 1498 (2006).
- [19] L. Verslegers, P. B. Catrysse, Z. Yu, and S. Fan, Deep-Subwavelength Focusing and Steering of Light in an Aperiodic Metallic Waveguide Array, *Physical Review Letters* **103**, 033902 (2009).
- [20] C. Li, R. Cui, F. Ye, Y. V. Kartashov, L. Torner, and X. Chen, Self-deflecting plasmonic lattice solitons and surface modes in chirped plasmonic arrays, *Optics Letters* **40**, 898 (2015).
- [21] M. J. Heck, Highly integrated optical phased arrays: photonic integrated circuits for optical beam shaping and beam steering, *Nanophotonics* **6**, 93 (2016).
- [22] P. B. Catrysse, V. Liu, and S. Fan, Complete power concentration into a single waveguide in large-scale waveguide array lenses, *Scientific Reports* **4**, 6635 (2014).
- [23] M. Wimmer, A. Regensburger, M.-A. Miri, C. Bersch, D. N. Christodoulides, and U. Peschel, Observation of optical solitons in PT-symmetric lattices, *Nature Communications* **6**, 7782 (2015).
- [24] P. A. Kalozoumis, C. V. Morfonios, F. K. Diakonov, and P. Schmelcher, PT-symmetry breaking in waveguides with competing loss-gain pairs, *Physical Review A* **93**, 063831 (2016).
- [25] S. Wu, W. Song, S. Gao, Y. Chen, S. Zhu, and T. Li, Floquet π mode engineering in non-hermitian waveguide lattices, *Physical Review Research* **3**, 023211 (2021), publisher: American Physical Society.
- [26] R. El-Ganainy, K. G. Makris, M. Khajavikhan, Z. H. Musslimani, S. Rotter, and D. N. Christodoulides, Non-Hermitian physics and PT symmetry, *Nature Physics* **14**, 11 (2018).
- [27] M. Kim, Z. Jacob, and J. Rho, Recent advances in 2d, 3d and higher-order topological photonics, *Light: Science & Applications* **9**, 130 (2020).
- [28] I. Cerutti, N. Andriolli, and P. Velha, Engineering of closely packed silicon-on-insulator waveguide arrays for mode division multiplexing applications, *Journal of the Optical Society of America B* **34**, 497 (2017).
- [29] H. Benisty, A. Lupu, and A. Degiron, Transverse periodic PT-symmetry for modal demultiplexing in optical waveguides, *Physical Review A* **91**, 053825 (2015).
- [30] M. Teimourpour, A. Rahman, K. Srinivasan, and R. El-Ganainy, Non-Hermitian Engineering of Synthetic Saturable Absorbers for Applications in Photonics, *Physical Review Applied* **7**, 014015 (2017).
- [31] M. Parto, S. Wittek, H. Hodaie, G. Harari, M. A. Bandres, J. Ren, M. C. Rechtsman, M. Segev, D. N. Christodoulides, and M. Khajavikhan, Edge-Mode Lasing in 1D Topological Active Arrays, *Physical Review Letters* **120**, 113901 (2018).
- [32] Y. Yang, R. J. Chapman, A. Youssry, B. Haylock, F. Lenzini, M. Lobino, and A. Peruzzo, Programmable quantum circuits in a large-scale photonic waveguide array, *npj Quantum Information* **11**, 19 (2025).
- [33] A. S. Solntsev, A. A. Sukhorukov, D. N. Neshev, and Y. S. Kivshar, Spontaneous Parametric Down-Conversion and Quantum Walks in Arrays of Quadratic Nonlinear Waveguides, *Physical Review Letters* **108**, 023601 (2012).
- [34] N. Matsuda, H. Nishi, P. Karkus, T. Tsuchizawa, K. Yamada, W. J. Munro, K. Shimizu, and H. Takesue, Generation of entangled photons using an arrayed waveguide grating, *Journal of Optics* **19**, 124005 (2017).
- [35] A. Raymond, A. Zecchetto, J. Palomo, M. Morassi, A. Lemaître, F. Raineri, M. Amanti, S. Ducci, and F. Baboux, Tunable Generation of Spatial Entanglement in Nonlinear Waveguide Arrays, *Physical Review Letters* **133**, 233602 (2024).
- [36] W. Cheng, W. Liu, Q. Liu, and F. Chen, Observation of topological Anderson phase in laser-written quasi-periodic waveguide arrays, *Optics Letters* **47**, 2883

- (2022).
- [37] U. Peschel, T. Pertsch, and F. Lederer, Optical Bloch oscillations in waveguide arrays, *Optics Letters* **23**, 1701 (1998).
- [38] N. Belabas, S. Bouchoule, I. Sagnes, J. A. Levenson, C. Minot, and J.-M. Moison, Confining light flow in weakly coupled waveguide arrays by structuring the coupling constant: towards discrete diffractive optics, *Optics Express* **17**, 3148 (2009).
- [39] A. P. Lara and S. Roy, Dynamic diffractive resonant radiation in a linearly chirped nonlinear waveguide array, *Physical Review A* **102**, 033512 (2020).
- [40] M. Honari-Latifpour, A. Binaie, M. A. Eftekhar, N. Madamopoulos, and M.-A. Miri, Arrayed waveguide lens for beam steering, *Nanophotonics* **11**, 3679 (2022).
- [41] D. Cai, A. R. Bishop, and N. Grønbech-Jensen, Localized states in discrete nonlinear schrödinger equations, *Physical Review Letters* **72**, 591 (1994).
- [42] D. N. Christodoulides and R. I. Joseph, Discrete self-focusing in nonlinear arrays of coupled waveguides, *Optics Letters* **13**, 794 (1988).
- [43] H. S. Eisenberg, Y. Silberberg, R. Morandotti, A. R. Boyd, and J. S. Aitchison, Discrete Spatial Optical Solitons in Waveguide Arrays, *Physical Review Letters* **81**, 3383 (1998).
- [44] R. Morandotti, H. S. Eisenberg, Y. Silberberg, M. Sorel, and J. S. Aitchison, Self-Focusing and Defocusing in Waveguide Arrays, *Physical Review Letters* **86**, 3296 (2001).
- [45] G. P. Agrawal, *Nonlinear fiber optics*, 5th ed., edited by G. P. Agrawal, Engineering professional collection (Academic, Oxford, 2013) includes bibliographical references and index.
- [46] T. X. Tran and F. Biancalana, Diffractive Resonant Radiation Emitted by Spatial Solitons in Waveguide Arrays, *Physical Review Letters* **110**, 113903 (2013).
- [47] A. Szameit, D. Blömer, J. Burghoff, T. Pertsch, S. Nolte, and A. Tünnermann, Hexagonal waveguide arrays written with fs-laser pulses, *Applied Physics B* **82**, 507 (2006).
- [48] J. Lv, Y. Cheng, W. Yuan, X. Hao, and F. Chen, Three-dimensional femtosecond laser fabrication of waveguide beam splitters in LiNbO₃ crystal, *Optical Materials Express* **5**, 1274 (2015).
- [49] I. Pavlov, O. Tokel, S. Pavlova, V. Kadan, G. Makey, A. Turnali, Ö. Yavuz, and F. Ö. Ilday, Femtosecond laser written waveguides deep inside silicon, *Optics Letters* **42**, 3028 (2017).
- [50] H. Wang, W. Zhang, D. Ladika, H. Yu, D. Gailevičius, H. Wang, C. Pan, P. N. S. Nair, Y. Ke, T. Mori, J. Y. E. Chan, Q. Ruan, M. Farsari, M. Malinauskas, S. Juodkazis, M. Gu, and J. K. W. Yang, Two-Photon Polymerization Lithography for Optics and Photonics: Fundamentals, Materials, Technologies, and Applications, *Advanced Functional Materials* **33**, 2214211 (2023).
- [51] J. W. Fleming, Dispersion in GeO₂-SiO₂ glasses, *Applied Optics* **23**, 4486 (1984).
- [52] R. Tewari and K. Thyagarajan, Analysis of tunable single-mode fiber directional couplers using simple and accurate relations, *Journal of Lightwave Technology* **4**, 386 (1986).
- [53] A. W. Snyder, Coupled-Mode Theory for Optical Fibers, *Journal of the Optical Society of America* **62**, 1267 (1972).
- [54] Y. Yang, R. J. Chapman, B. Haylock, F. Lenzini, Y. N. Joglekar, M. Lobino, and A. Peruzzo, Programmable high-dimensional Hamiltonian in a photonic waveguide array, *Nature Communications* **15**, 50 (2024).
- [55] H. S. Eisenberg, Y. Silberberg, R. Morandotti, and J. S. Aitchison, Diffraction management, *Physical Review Letters* **85**, 1863 (2000).
- [56] Z. Cao, X. Qi, G. Zhang, and J. Bai, Asymmetric light propagation in transverse separation modulated photonic lattices, *Optics Letters* **38**, 3212 (2013).
- [57] D. Anderson, F. Cattani, and M. Lisak, On The Pereira-Stenflo Solitons, *Physica Scripta* **T82**, 32 (1999).
- [58] D. Marcuse, Gaussian approximation of the fundamental modes of graded-index fibers, *Journal of the Optical Society of America* **68**, 103 (1978).
- [59] M. Karlsson, D. Anderson, and M. Desaix, Dynamics of self-focusing and self-phase modulation in a parabolic index optical fiber, *Optics Letters* **17**, 22 (1992).
- [60] G. P. Agrawal, *Physics and Engineering of Graded-Index Media* (Cambridge University Press, 2023).
- [61] T. Hansson, A. Tonello, T. Mansuryan, F. Mangini, M. Zitelli, M. Ferraro, A. Niang, R. Crescenzi, S. Wabnitz, and V. Couderc, Nonlinear beam self-imaging and self-focusing dynamics in a GRIN multimode optical fiber: theory and experiments, *Optics Express* **28**, 24005 (2020).
- [62] I. E. Papacharalampous, P. G. Kevrekidis, B. A. Malomed, and D. J. Frantzeskakis, Soliton collisions in the discrete nonlinear schrödinger equation, *Physical Review E* **68**, 046604 (2003), 00091.
- [63] A. P. Lara and S. Roy, Collision dynamics of a discrete soliton in uniform waveguide arrays, *Journal of the Optical Society of America B* **40**, 594 (2023).
- [64] A. A. Sukhorukov and Y. Kivshar, Generation and stability of discrete gap solitons, *Optics Letters* **28**, 2345 (2003).
- [65] D. E. Pelinovsky, Y. S. Kivshar, and V. V. Afanasjev, Internal modes of envelope solitons, *Physica D: Nonlinear Phenomena* **116**, 121 (1998).